Available online at www.sciencedirect.com
ScienceDirect
Polymer 48 (2007) 4733–4741
polymer
www.elsevier.com/locate/polymer

Photo-initiated polymerization of acrylamide in water

Shane A. Seabrook [a], Robert G. Gilbert [b,*]

[a] Key Centre for Polymer Colloids, School of Chemistry F11, The University of Sydney, NSW 2006, Australia
[b] LCAFS/CNAFS, University of Queensland, Brisbane, Qld 4072, Australia

Received 8 April 2007; received in revised form 7 June 2007; accepted 7 June 2007
Available online 15 June 2007

Abstract

The kinetics of the photo-initiated polymerization of acrylamide in water, at up to 10% w/w polymer and under ambient conditions, are studied using in situ Raman spectroscopy. Three photo-initiators were studied, UO_2^{2+}, 2,2′-azobis(2-amidinopropane) (''V-50'') and persulfate, with photo-initiation by a low-pressure Hg lamp. The dependences of polymerization rate on time, initiator concentration and initiator type show that classical free-radical polymerization kinetics provides an acceptable quantitative description for this system, even though the rate coefficients controlling aqueous-phase polymerization of acrylamide are very sensitive to changes in solvency during polymerization. The initiation rates with all three photo-initiators were proportional to the absorption at 254 nm wavelength of the Hg lamp.

Keywords: Acrylamide; Free-radical polymerization; Photo-initiation

1. Introduction

Polymers containing water-soluble monomers such as acrylamide and acrylic acid have many industrial applications [1]. The rate coefficients for the various processes involved in the free-radical polymerization of water-soluble monomers in the aqueous phase are very sensitive to solvent effects, such as the concentrations of monomer, polymer and initiator (e.g. Refs. [2–6]). This sensitivity can be understood in terms of the sensitivity of the energies of reactants and transition state to polar effects [7], but cannot yet be predicted ab initio with sufficient accuracy. An additional complexity is afforded by the chain-length dependence of the termination rate coefficient, an effect present in all free-radical polymerizations.

One case of technical importance where this complexity may be reduced is the polymerization of acrylamide in water solutions at moderate concentrations, say up to 10% monomer. Solution polymerization of relatively dilute polymer (~10%) is not infrequently used to produce gels for sodium dodecyl sulfate polyacrylamide gel electrophoresis (SDS–PAGE), a widely used technique for identifying proteins and their substructures in biomedicine and agriculture (e.g. Ref. [8]). SDS–PAGE membranes comprise polyacrylamide cross-linked with bisacrylamide. Photo-activated polymerization under ambient conditions is used to produce these membranes; the membranes have a large surface area which is not sealed and are formed on a substrate which does not allow a heat-initiated or redox polymerization to be set in place.

The objective of the present study is to examine the kinetics of photo-induced free-radical polymerization of acrylamide under similar conditions to those used to produce SDS–PAGE membranes, but without cross-linking agent. The relatively low levels of cross-linking in typical commercial recipes should not have any significant kinetic effect on the overall polymerization rate because all rate processes in this system are either under chemical control or governed by diffusion of small entities; neither chemically controlled nor (oligomeric) diffusion-controlled reactions will be affected significantly by a few cross-links in a polymer/solvent matrix.

The present study aims to find the rate 'laws' controlling photo-initiated polymerization of acrylamide under conditions similar to those used in industry to make some widely used

* Corresponding author. Tel.: +61 7 3365 4809; fax: +61 7 3365 1188.
E-mail address: b.gilbert@uq.edu.au (R.G. Gilbert).

0032-3861/$ - see front matter © 2007 Elsevier Ltd. All rights reserved.
doi:10.1016/j.polymer.2007.06.020

SDS–PAGE membranes. The total monomer/polymer concentration being low, classical kinetics should provide a good starting point for kinetic analysis; however, the effects of changes in solvency and of chain-length dependent termination are sufficiently strong in this system; it is anticipated that an accurate quantitative description of the polymerization kinetics would need significant improvements upon the classical model. Indeed, deviations from classical kinetics for acrylamide polymerization are apparent in the literature (e.g. Ref. [9]).

There have been quite a few studies of the free-radical polymerization of acrylamide in solution under a wide range of conditions (going back to the pioneering work of Dainton and colleagues [10–13]). As reviewed by Lalot et al. [14], previous studies [15–19] interpreted rate data in terms of quantities such as an empirical exponent describing the dependence of rate on monomer and initiator concentrations. No study has been made where an attempt was made to separate the various terms in the expression for the polymerization rate, $k_p[M][R^\bullet]$, where [M] and [R•] are the concentrations of monomer and radicals, respectively. This separation has only recently become possible with the advent of pulsed-laser polymerization data for k_p of acrylamide, and in particular data showing its (strong!) dependence on monomer concentration and ionic strength [6]. The availability of appropriate k_p data now should make it possible to separate (a) how initiator and monomer concentrations affect k_p (for reasons that are now understood from basic theory [7]) from (b) whatever kinetic and thermodynamic quantities affect [R•]. The availability of k_p data thus replaces an empirical analysis of the reaction order with respect to monomer and initiator concentrations, which is the only data treatment applied hitherto to acrylamide solution polymerization. Moreover, there have been no detailed polymerization rate studies under the particular conditions used for synthesis of some widely used protein-analysis membranes.

In the present study, a reactor system is chosen which is similar to those used for making such membranes. Polymerization is monitored by real-time Raman spectroscopy (e.g. Ref. [20]). A simple one-component photo-initiator is used, rather than the complex three-component system developed by Righetti et al. [21] in the early 1980s that utilizes a riboflavin-based catalyst as well as a photo-decomposable component. The present photo-initiators are 2,2′-azobis(2-amidinopropane) (V-50), the uranyl ion [22] and persulfate.

2. Experimental

2.1. Materials

Acrylamide (Electrophoresis grade, Sigma Aldrich, 99.9%), 2,2′-azobis(2-amidinopropane) (“V-50” from Wako Chemicals, 99%), uranyl nitrate (Ajax Chemicals, 99%) and potassium persulfate (Sigma Aldrich, 99%) were all used as received. Milli-Q water (Milli-Q plus) was used in all instances. Polymerizations were conducted on aluminium foil plates; although these do not exactly replicate a normal hydrogel substrate, they are ideal for reflecting Stokes-Raman signal back into the Raman probe. Control polymerizations were conducted on glass plates to assess whether the aluminium metal interfered with the polymerization rate or altered the inhibition period. Polymerization profiles in both cases were essentially identical. Nitrogen gas (BOC Gas, ultra pure) was used in all cases.

2.2. Polymerization

The aqueous solutions of acrylamide (AAm) were filtered with a Durapore poly(vinylidene fluoride) of 0.45 μm filter. The addition of photo-initiator to the AAm solution was conducted in an unlit fume hood in an attempt to minimize photodissociation. In each case double/triple the quantity required for a single run was prepared, allowing duplicate/triplicate polymerizations to be conducted. Prior to polymerization the samples *were not* purged with N_2, so as to mimic a typical industrial procedure; O_2 acts as a very effective inhibitor. Once sample solutions were transferred to an appropriate reaction medium, they were placed inside a poly(methyl methacrylate) reactor that contained an initiation source, the Raman probe and a positive pressure of N_2. Nitrogen was flushed through the samples for 10 min prior to activation of the UV source.

All polymerizations were conducted at ambient temperature (~20 °C) using 1.41 M AAm, which corresponds to 10% monomer in water (w/v). This concentration is typical of an industrial polymerization. Signals were collected from 1% to 10% w/w polymer concentrations.

2.3. Dispersive Raman spectroscopy

Monitoring of conversion was through the use of a Renishaw Raman System 2000 Ramanscope (Renishaw Plc., Wotton-under-Edge, UK), equipped with an air-cooled charge-coupled device (CCD) camera as remote probe. The attached microscope was a Leica DMLM equipped with a 10× objective which is optimized for use with the fiber-optic coupling used to obtain scattering signal from the remote probe, and a trinocular viewer which accommodates a video camera allowing high resolution focus of the fiber-optic couple via an image viewer. Sample excitation was achieved using a Stabilite 2017 argon ion laser at 514 nm (Spectra-Physics, CA, USA) at an energy of 40 mW. Calibration of the instrument before use was achieved by recording the Raman spectrum of Si using one accumulation of 10 s. An offset correction was performed on the grating to ensure that the position of the silicon band is 520.50 cm^{-1}. The spectrometer was controlled using two software packages, one for instrument control (WiRE™ Version 1.3.18, Renishaw Plc., Wotton-under-Edge, UK) and the other for data analysis (GRAMS/32® Version 4.14 Level II, Galactic Industries Corporation, Salem, USA). An sample spectrum is shown in Fig. 1. The peaks of significant interest are the symmetric water shift at 3360 cm^{-1} which is used for signal normalization, and the vinyl CH_2 shift at 1285 cm^{-1} used for monitoring the concentration of AAm.

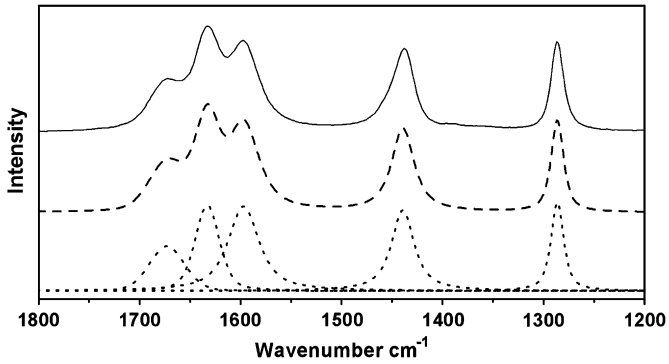

Fig. 1. Dispersive Raman spectrum of AAm and polyacrylamide (top) during polymerization, deconvoluted (middle and bottom spectra) to obtain the integral of the peak at 1285 cm^{-1}, which is a monomer CH_2 stretching vibration. The bottom panel shows the separate deconvoluted peaks, whose sum gives the middle panel, which is essentially indistinguishable from the actual spectrum in the top panel.

2.4. Remote Raman analysis

Dispersive Raman spectroscopy utilized an in-built filter grating and lens with a focal distance of 22 mm. The excitation beam from a Stabilite 2017 argon ion laser was fed into the probe via a 5 m fiber-optic cable using an OzOptics fiber-optic coupling device. This device captures 100% of the excitation beam and as such only a small amount of excitation laser power is lost over 5 m (typically less than 20%). The scattered signal was directed back via a separate optic–optic cable and mounted on the microscope stage using an OzOptics microscope coupler. A schematic of reactor and probe is shown in Fig. 2.

Each polymerization was set to collect 100 spectra (requiring ~2 h in total) using the static-mapping function of GRAMS/32 with a collection time of 10 s for each spectrum (without accumulation). Smoothing was accomplished by Fourier transforming the data using a triangular filter function applied with the apodization value reaching zero at a specific cutoff point controlled by the percentage-of-smoothing variable; a value of 10% was found to produce spectra with significantly less noise and no additional spectral artifacts. After smoothing, each spectrum was baseline corrected using a series of points forced on the data at 4000, 2500, 1800, 1200 and 400 cm^{-1} (the intensity at these wave numbers was found to remain unchanged over the course of a polymerization) set to zero intensity with a linear baseline. Each spectrum was normalized using a water peak, the symmetric OH shift at 3360 cm^{-1}. A typical spectrum at the region used for analysis is shown in Fig. 3.

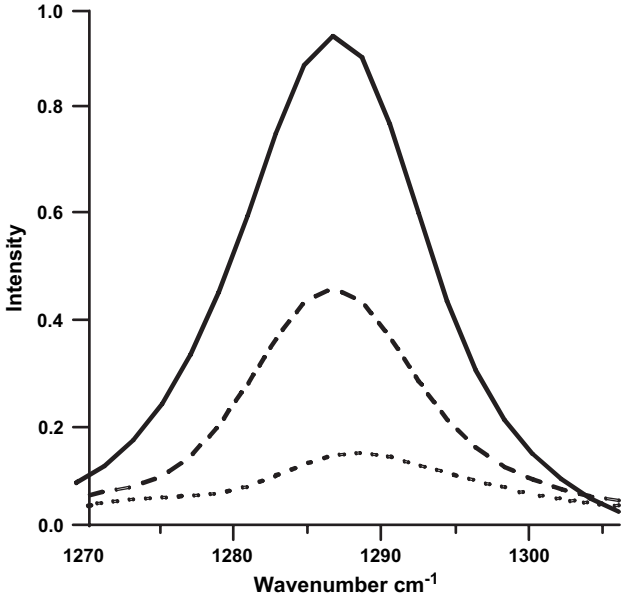

Fig. 3. Normalized Raman intensity of the monomer peak during photo-initiated polymerization with 6.9 mM persulfate at 16, 35 and 90 min.

3. Results

As stated, the starting point for data representation will be classical free-radical kinetics. The low-pressure mercury lamp used here has sharp emission lines, and those of potential relevance for the present system are at 254 and 365 nm. For photo-initiation in the case of low absorption (low

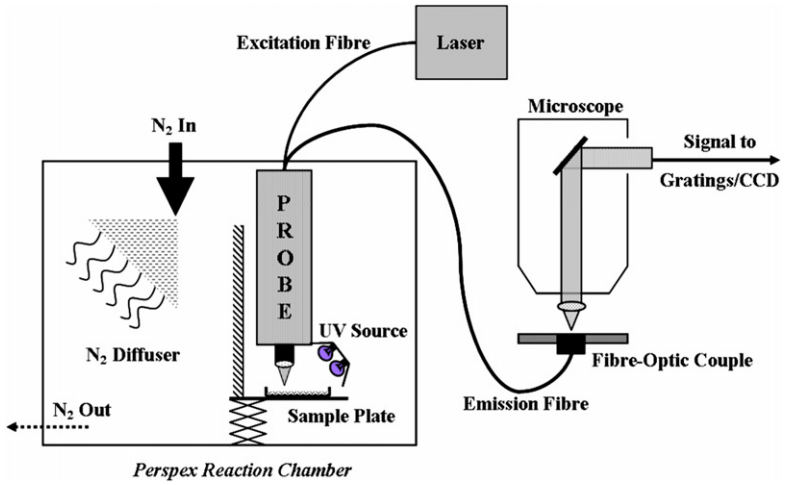

Fig. 2. Schematic representation of the Raman probe and reactor system.

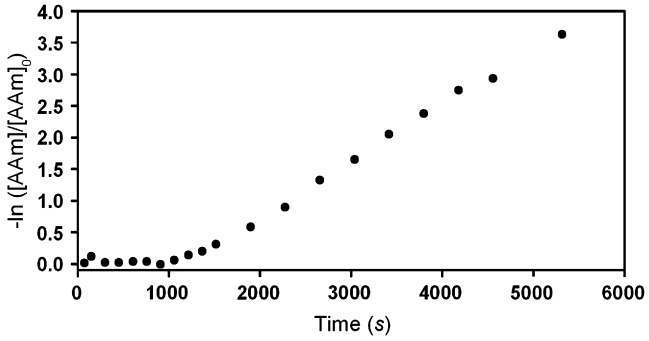

Fig. 4. Fractional conversion, as $\ln[M]/[M]_0$, of 10% (1.41 M) water solution of AAm and 0.0069 M potassium persulfate photo-initiator.

concentration of photo-initiator I), the rate of radical production, $d[R^\bullet]/dt$, at a given wavelength is given by

$$\frac{d[R^\bullet]}{dt} = F\varepsilon\Phi[I] \quad (1)$$

where F is the photon flux, ε the (wavelength-dependent) molar extinction coefficient (which is the same as the absorption cross-section in appropriate units) and Φ the (wavelength-dependent) efficiency (which allows for geminate recombination of initiator). With classical free-radical polymerization kinetics, the polymerization rate is given by

$$R'_p = \frac{-d\ln([M]/[M]_0)}{dt} = \left(\frac{F\varepsilon\Phi k_p^2}{k_t}\right)^{0.5}[I]^{0.5} \quad (2)$$

Here k_t is the termination rate coefficient, $[M]$ = monomer concentration at time t, and $[M]_0$ = initial monomer concentration. If classical kinetics are applicable, $\ln([M]/[M]_0)$ should

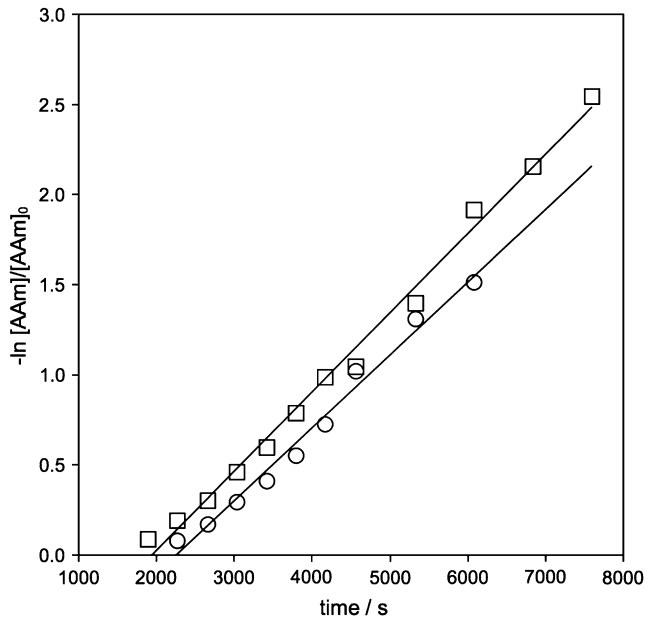

Fig. 5. Fractional conversion, as $\ln[M]/[M]_0$, for replicate polymerizations of 10% AAm with 0.0011 M potassium persulfate photo-initiator; induction period not shown. Straight lines are least-squares fits.

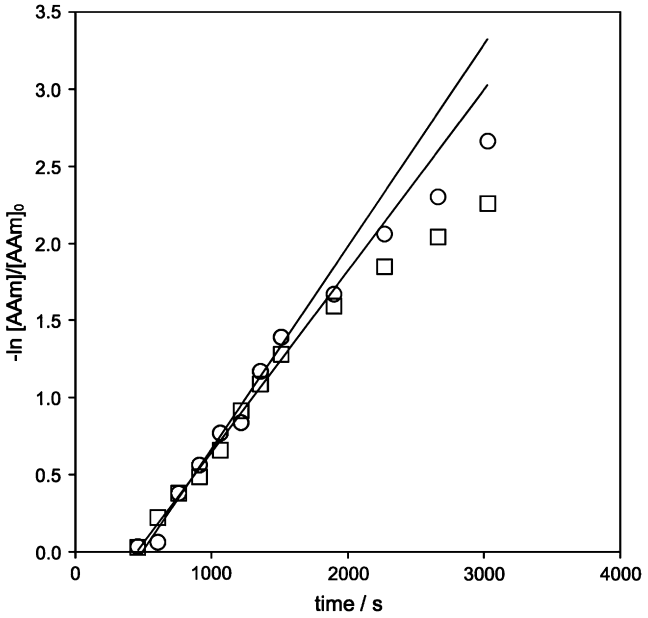

Fig. 6. Fractional conversion, as $\ln[M]/[M]_0$, for replicate polymerizations of 10% AAm with 0.0010 M uranyl nitrate photo-initiator; induction period not shown. Straight lines are least-squares fits to data for times $\leq$ 1500 s.

be linear in time, after an induction period. Examples, including replicate runs, are shown in Figs. 4–7 and all results summarized in Table 1.

Persulfates are not typically used for photo-initiation, and the small but significant photo-initiated polymerization rate with this initiator was initially surprising, as persulfate has very weak absorption of UV-A light. To confirm that this was not due to some artifact, a control polymerization was conducted with 0.01 M persulfate and 1.41 M AAm without

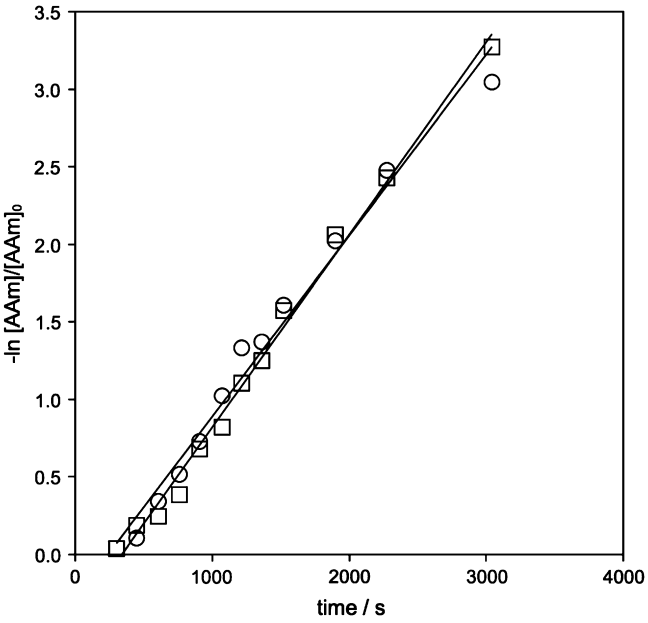

Fig. 7. Fractional conversion, as $\ln[M]/[M]_0$, for replicate polymerizations of 10% AAm with 0.0100 M V-50 photo-initiator; induction period not shown. Straight lines are least-squares fits.

Table 1
Induction times and rates from the photo-initiated polymerization of 10% acrylamide solution in water

Initiator type	Concentration (mM)	R'_p (s^{-1})	Induction time (s)
V-50	0.50	3.3×10^{-4}	600
V-50	0.50	2.8×10^{-4}	750
V-50	1.0	5.3×10^{-4}	750
V-50	1.0	5.1×10^{-4}	750
V-50	5.0	1.0×10^{-3}	300
V-50	5.0	1.1×10^{-3}	300
V-50	10.0	1.2×10^{-3}	450
V-50	10.0	1.3×10^{-3}	300
V-50	10.0	1.2×10^{-3}	450
V-50	10.0	1.0×10^{-3}	300
Uranyl nitrate	0.60	6.2×10^{-4}	750
Uranyl nitrate	0.60	6.1×10^{-4}	900
Uranyl nitrate	0.50	6.2×10^{-4}	600
Uranyl nitrate	0.50	5.7×10^{-4}	600
Uranyl nitrate	0.70	8.4×10^{-4}	450
Uranyl nitrate	0.70	7.9×10^{-4}	300
Uranyl nitrate	1.00	9.8×10^{-4}	500
Uranyl nitrate	1.00	8.7×10^{-4}	500
Uranyl nitrate	5.0	1.2×10^{-3}	300
Uranyl nitrate	5.0	1.4×10^{-3}	300
Uranyl nitrate	5.0	1.3×10^{-3}	500
Uranyl nitrate	10.0	1.5×10^{-3}	150
Uranyl nitrate	10.0	1.2×10^{-3}	200
KPS	1.10	4.1×10^{-4}	1900
KPS	1.10	3.5×10^{-4}	1900
KPS	5.0	6.2×10^{-4}	1000
KPS	5.0	7.9×10^{-4}	700
KPS	6.9	8.3×10^{-4}	900
KPS	10.0	1.1×10^{-3}	200
KPS	10.0	9.9×10^{-4}	200

The values for the rate, R'_p, are the slopes of the linear region of the $d(-\ln([AAm]/[AAm_0])/dt$ plots.

the UV light source to assess if initiation was occurring by another mechanism (perhaps thermal). The concentration of unreacted AAm remained constant to 7200 s (100 spectra collection), indicating that the UV light source was necessary to initiate polymerization.

3.1. Induction period

All runs show a significant induction period which is not highly reproducible in replicate runs. This is expected in a system where, to imitate typical industrial systems, removal of oxygen was not rigorous (see Section 2). The induction time in a series of runs which had identical initial concentrations of inhibitor $[Inhib]_0$ would be given by $[Inhib]_0/R_i$, where R_i is the initiation rate [23], which in turn would be expected to be proportional to the concentration of photo-initiator. Fig. 8 shows a plot of induction times as a function of $[I]^{-1}$ for each of the three photo-initiators. Although a general trend of decreasing induction time with increasing initiator concentration is seen, no quantitative conclusions can be drawn from these data, because of the scatter in the inhibition times for replicate runs.

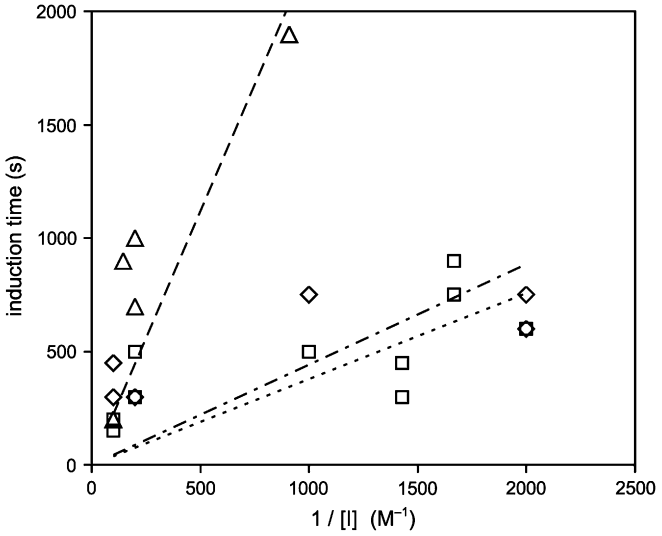

Fig. 8. Induction times as a function of the reciprocal of photo-initiator concentration for V-50 (◇), uranyl nitrate (□), KPS (△). Lines are least-squares fits forced to pass through the origin: KPS — — —; V-50 — · — · ; uranyl nitrate - - -.

3.2. Rate data and applicability of classical free-radical kinetics

Figs. 5–7 show the data and a least-squares fit to the classical expression for the rate, Eq. (2), i.e. fitting a straight line to $\ln[M]/[M]_0$ as a function of time. All data in Figs. 5–7, and corresponding data for all the runs given in Table 1, show a good linear fit except for higher concentrations of UO_2^{2+}, where (as illustrated in Fig. 6) linearity is only obtained at early times. Thus the linearity in $-\ln([AAm]/[AAm_0])$ with time expected from classical kinetics (after the induction period) is seen in all cases except at higher conversions for higher concentrations of UO_2^{2+}.

There are two possible causes for the non-linearity at higher UO_2^{2+} concentrations.

(1) The first is the chain-length dependence of the termination rate coefficient. Termination is dominated by reactions between mobile short radicals and less mobile long ones [24–27]; this effect starts to decrease the rate as conversion increases and the diffusion coefficients of shorter radicals thus decrease. However, the data of Fig. 6 show immediately that this cannot be the origin of the non-linearity, because chain-length dependent termination is predicted to give an *increase* in polymerization rate, whereas the observed non-linearity is actually in the form of a rate *decrease*. Moreover, this non-linearity is not seen with the other photo-initiators at concentrations showing similar polymerization rates, showing that changes in rate due to chain-length dependence of k_t alone cannot be responsible for the non-classical behaviour in rate for higher concentrations of uranyl nitrate. The effects of chain-length dependent termination are discussed in a subsequent section.

(2) The second possible origin is changes in any of the rate coefficients as solvency changes during conversion; as noted

above, all rate coefficients in the aqueous-phase free-radical polymerization of water-soluble monomers have either been shown to, or are expected to, exhibit a strong dependence on solvent. Indeed, we have shown that uranyl nitrate at the concentration shown in Fig. 6 gives a significant decrease in the k_p of AAm compared to the value at lower ionic strengths, and it would not be unexpected for the change in solvency during conversion of monomer to polymer to lead to changes in one or more rate coefficients which could lead to the observed rate decreases.

It has been pointed out on several occasions in the literature that there is a need for further investigations into these solvent effects. For the present purposes, it is sufficient to note that this effect is relatively small in the particular system studied here (a 10% solution of monomer), and that even for high concentrations of UO_2^{2+}, linear behaviour is observed at lower conversion.

Eq. (2) suggests that if classical kinetics are applicable, the polymerization rate for a given photo-initiator should be proportional to $[I]^{1/2}\varepsilon^{1/2}$, ε being the extinction coefficient of the photo-initiator at the wavelength at which radicals are produced. Plotting each species of photo-initiator separately for clarity, it is observed from Figs. 9–11 that there is indeed an approximately linear relationship between R'_p and the square root of the photo-initiator concentrations (except at the highest ionic strengths), which leads to the conclusion that the rate behaviour of the AAm systems under consideration here is consistent with classical kinetics.

The slope of these plots of R'_p against $[I]^{1/2}$ is denoted as S. Eq. (2) also suggests that if classical kinetics are applicable to this photo-initiation system, a plot of S against $\varepsilon^{1/2}$, at the wavelength at which radicals are produced, should be linear. The UV absorption spectra for the three photo-initiators are shown in Fig. 12. Fig. 13 shows plots of S against $\varepsilon^{1/2}$ (as relative absorbance) for the three photo-initiators at two Hg wavelengths of possible importance in the present system: the prominent one in the UV-A light range, 254 nm, and the less intense one in the UV-C light range, 365 nm. Both V-50 and uranyl nitrate show extensive absorption at the UV-C wavelength, while all the three show significant absorption at the UV-A wavelength.

Comparing the dependences on the two wavelengths in Fig. 13, it is seen that Eq. (2) is valid for an excitation wavelength of 254 nm, but not for 365 nm. It is apparent that, not surprisingly, most photo-initiation is at the shorter wavelength. Again, the data are consistent with classical free-radical polymerization kinetics.

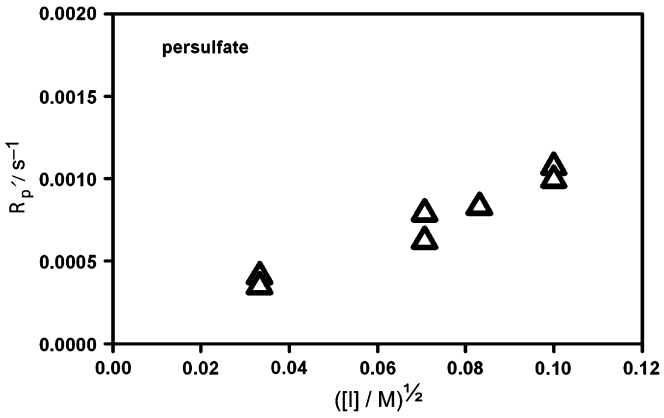

Fig. 9. R'_p as a function of the square root of persulfate concentration.

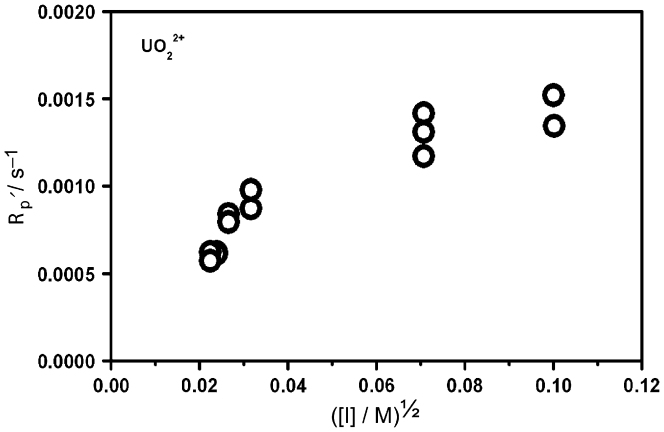

Fig. 10. R'_p as a function of the square root of uranyl nitrate concentration.

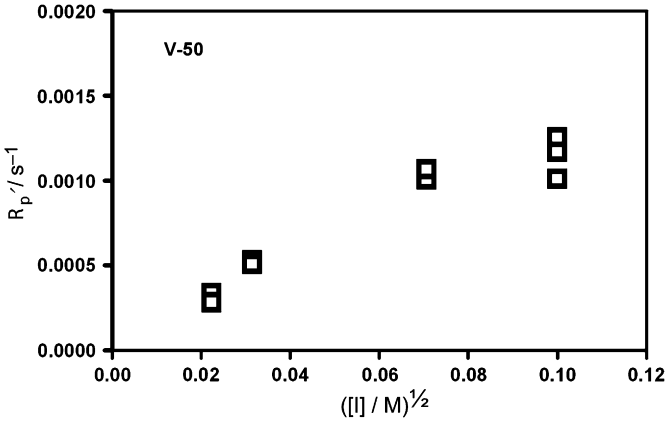

Fig. 11. R'_p as a function of the square root of V-50 concentration.

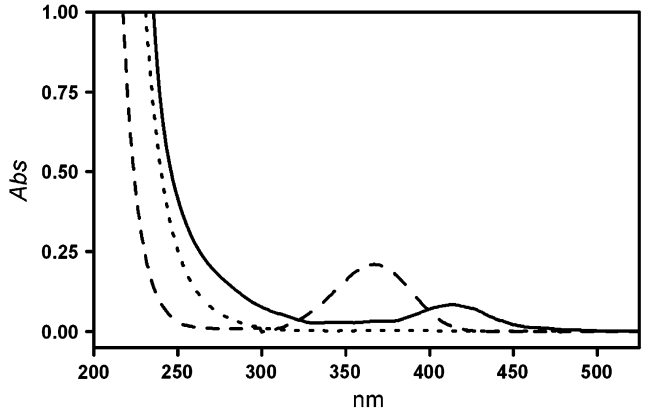

Fig. 12. UV absorption spectrum of 0.001 M uranyl nitrate (solid), 0.001 M V-50 (dashed line) and 0.01 M potassium persulfate (dotted line).

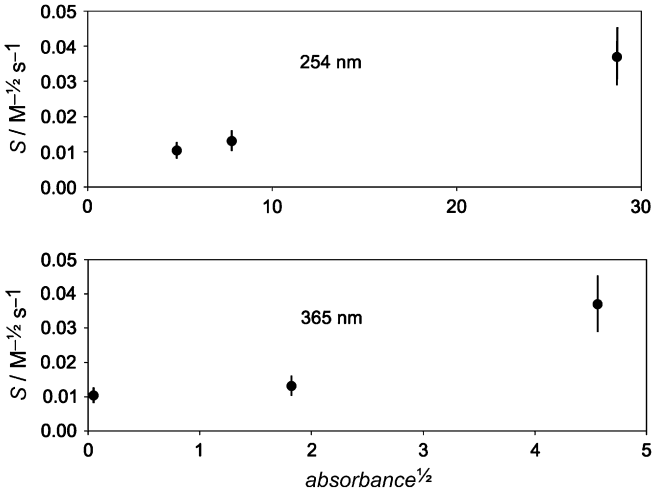

Fig. 13. Dependence of slope S of Figs. 9–11 on absorbance of each photoinitiator at the two Hg wavelengths.

While data of the type shown in Fig. 13 could be used to infer the cross-section for photodissociation, this was not implemented here, because the present set-up, being similar to the system typically used industrially, does not have spatially uniform illumination.

3.3. Why is classical kinetics valid?

It is apparent from the results given above that classical free-radical polymerization kinetics furnish an adequate description of most of the rate data. However, it is well established that the termination rate coefficient is chain-length dependent, and thus the average termination rate coefficient changes with conversion. Moreover, the propagation rate coefficient of AAm depends on the concentration of free monomer [6]. The question therefore arises as to whether current theoretical and experimental knowledge of the various component rate coefficients in the overall kinetics of conversion for this system is consistent with the observed behaviour.

One issue relevant to this question is whether the concentration range is dilute, semi-dilute or concentrated. While no molecular weight and viscosity data were obtained in the present study to provide a direct answer to this question, modelling with the parameters discussed below shows that number-average molecular weights are well above 10^6; using literature values [28] of the expansion factor ($\sim$2.6) and the characteristic ratio ($\sim$15) yields a calculated value of the critical overlap concentration of $\sim$0.4% for a molecular weight of 10^6; since critical entanglement concentrations are not grossly larger than critical overlap concentrations, it is highly likely that virtually all of the polymerization under the present conditions took place with entangled chains.

Complete simulations of the rate of polymerization of the present system were performed using standard methods by taking into account chain-length dependent termination [24,25,27,29–33]. The chain-length averaged termination rate coefficient, $\langle k_t \rangle$, including its dependence on fraction conversion, was found from the parameterization obtained using data [34] obtained by the direct determination of this quantity at 50 °C using γ relaxation experiments (with an exponent of 0.5 used for the empirical scaling relationship), and scaling the rate coefficients to 20 °C by simulating $\langle k_t \rangle$ from chain-length dependent k_t values calculated from the diffusion model [24,33] using standard methods [35]; the temperature difference was taken into account by assuming the same activation energy for diffusion coefficients as measured for another polar monomer, hydroxyethyl methacrylate [36]. The dependence of k_p on conversion (expressed as weight-fraction polymer, w_p) was taken from a pulsed-laser polymerization study [6], assuming that the concentration of polymer does not affect k_p. The (smoothed) dependences of k_p and $\langle k_t \rangle$ so obtained are shown in Fig. 14. The rate coefficient for transfer to monomer, k_{tr}, at 20 °C was taken to be 3.1 M^{-1} s^{-1}, an estimate made by scaling from that at 50 °C [34] assuming the activation energy for the transfer constant was the same as that for transfer to monomer in butyl acrylate (15.2 kJ mol^{-1}) [37]. The radical initiation rate was then obtained for each initiator by fitting

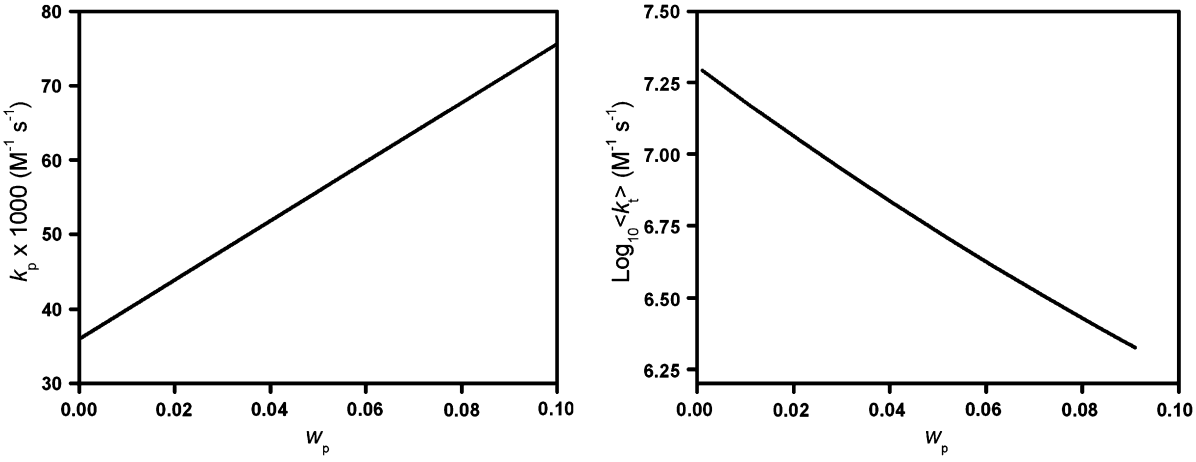

Fig. 14. Dependences of the apparent propagation rate coefficient, k_p, and the chain-length average termination rate coefficient, $\langle k_t \rangle$, as functions of the weight-fraction polymer, w_p, obtained as described in the text.

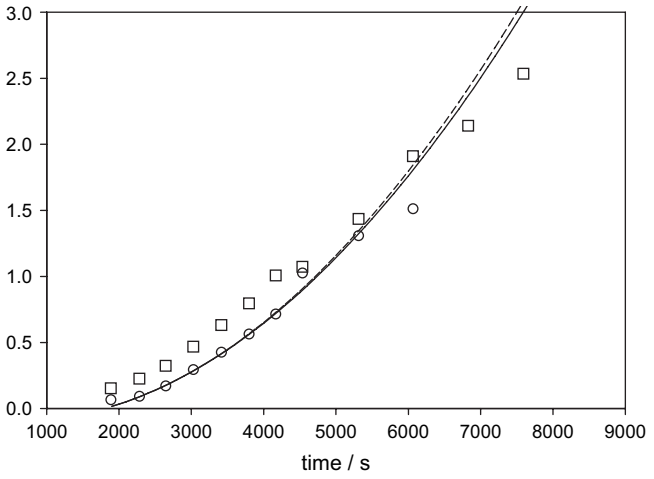

Fig. 15. Comparison between simulated (lines: full = k_p varying with w_p, broken = constant k_p) and experimental (replicate) time dependences of conversion for 10% AAm using 0.0011 M potassium persulfate (circles and squares).

to the present lowest-conversion rate data using the k_p and $\langle k_t \rangle$ parameter values.

These parameterizations were used to simulate the polymerization kinetics using conventional numerical solution of the appropriate rate equations. A typical result is shown in Fig. 15. Given that the parameterization of the initiation rate was chosen to fit the observed rate of polymerization at low conversion, it is apparent that the simulated rate of polymerization does not provide an accurate fit of the experimentally observed R'_p at later time. The simulations predict a significant dependence of the rate on conversion, a dependence which is not seen experimentally. There are some justifiable changes in the choice of parameters in the simulation: for example, one could argue that k_p might be independent of w_p for this system, because the experimental w_p dependence used to calculate that shown in Fig. 14 was obtained from experimental k_p values for a system without any polymer present, only with varying monomer concentration. However, as seen in Fig. 15, this change does not make any significant difference. It is only possible to choose values of the simulation parameters to force agreement with experiment if the dependence of the termination rate coefficient on chain length in these conditions of low polymer concentration is less than predicted by current models. These models have really only been thoroughly checked against data at much higher polymer concentrations.

There is no obvious reason why what should be a more sophisticated model actually affords a poorer approximation to the observed rate data than that afforded by classical kinetics. There are several possibilities, some or all of which may be operative. (1) The empirical scaling law for the chain-length dependence of diffusion of oligomeric radicals used to calculate $\langle k_t \rangle$ is based on data obtained above the critical overlap concentration c^*, and the present system includes data significantly below that concentration. (2) Scaling laws for diffusion coefficients of oligomers may well change near c^* [36]. (3) The dependences of k_p and $\langle k_t \rangle$ on w_p were obtained from systems where the polymer concentrations, which are also likely to affect the solvency and thus the rate coefficients, were different from the present one. (4) No attempt was made to account for possible dependence of k_{tr} on w_p, because no data for this dependence are available. (5) There are insufficient data to account for the dependences of all these quantities on ionic strength. (6) In particular, separation of terms in the rate expression $k_p[M][R^\bullet]$ requires measurement of k_p under conditions of the actual system, i.e. in the presence of polymer as well as monomer and other aqueous species. (7) Many of the extrapolations or assumptions required to estimate some of the parameters required for the simulation have not been tested.

4. Conclusions

The photo-initiated polymerization of acrylamide (at up to 10% w/v in water) was found to be well approximated by classical free-radical polymerization kinetics. Current models for this process predict that in fact classical kinetics should not be accurate for this system. There are many possible reasons for this failure of more sophisticated models, which shows the need to obtain more data on the various component rate coefficients (termination, propagation and transfer) on monomer, polymer and salt concentrations, and the chain-length dependences of k_t, in this concentration regime. These dependences are all both significant and beyond current fundamental theories, because of the high sensitivity of all the fundamental rate coefficients to solvent effects in the polymerization of polar monomers in water.

For the pragmatic goal of improving current methods used to make acrylamide-based gels for products such as SDS–PAGE, the (unexplained) applicability of classical kinetics in the region of industrial importance is in actuality an advantage. The data and data treatment given in the present paper shows that a simple measurement of the absorption spectrum of a photo-initiator is all that is needed to model its rate behaviour. What could be an extremely complex system to model is found, in a regime of considerable practical interest, to be very simple.

Acknowledgements

The support of an Australian Research Council Linkage (APA-I) and ARC LIEF grants are gratefully acknowledged, as are interactions with Dr. David Solomon, Dr. David Ogle of Life Therapeutics, and constructive comments from Assoc. Prof. Greg Russell and Dr. Chris Fellows. We greatly appreciate the aid of Dr. Elizabeth Carter of the University of Sydney for the in situ Raman spectroscopy.

References

[1] Urban D, Takamura K. Polymer dispersions and their industrial applications. Weinheim: Wiley-VCH; 2002.
[2] Kabanov VA, Topchiev DA, Karaputadze TM. J Polym Sci Polym Symp 1973;42:173.
[3] Blackley DC, Andries S, Sebastian RD. Br Polym J 1989;21:313.

[4] Lacik I, Beuermann S, Buback M. Macromolecules 2003;36:9355.
[5] Lacik I, Beuermann S, Buback M. Macromol Chem Phys 2004;205: 1080.
[6] Seabrook SA, Tonge MP, Gilbert RG. J Polym Sci Part A Polym Chem 2005;43:1357.
[7] Thickett SC, Gilbert RG. Polymer 2004;45:6993.
[8] Hames BD, editor. Gel electrophoresis of proteins: a practical approach. Oxford: Oxford University Press; 1998.
[9] Giz A, Catalgil-Giz H, Alb A, Brousseau J-L, Reed WF. Macromolecules 2001;34:1180.
[10] Collinson E, Dainton FS, McNaughton GS. Trans Faraday Soc 1957;53: 476.
[11] Collinson E, Dainton FS, McNaughton GS. Trans Faraday Soc 1957;53: 489.
[12] Dainton FS, Tordoff M. Trans Faraday Soc 1957;53:499.
[13] Dainton FS, Tordoff M. Trans Faraday Soc 1957;53:666.
[14] Lalot T, Brigodiot M, Marechal E. Polym Int 1999;48:288.
[15] Beylerian NM, Ruckenstein E, Harutyunyan RS, Grigoryan JD, Grigoryan VV, Hagopyan RM, et al. Oxid Commun 2002;25:383.
[16] Misra GS, Bhattacharya SN. J Polym Sci Polym Chem Ed 1982;20:131.
[17] Narain H, Jagadale SM, Ghatge ND. J Polym Sci Polym Chem Ed 1981; 19:1225.
[18] Riggs JP, Rodriguez F. J Polym Sci Polym Chem Ed 1967;5:3151.
[19] Chavez SL, Rodriguez F. Chem Eng Commun 1983;24:21.
[20] Baldock C, Rintoul L, Keevil SF, Pope JM, George GA. Phys Med Biol 1998;43:3617.
[21] Righetti PG, Gelfi C, Bosisio AB. Electrophoresis 1981;2:291.
[22] Venkatarao K, Santappa M. J Polym Sci Part A-1 Polym Chem 1970;8: 3429.
[23] Odian G. Principles of polymerization. 4th ed. Hoboken, NJ: Wiley Interscience; 2004.
[24] Russell GT, Gilbert RG, Napper DH. Macromolecules 1992;25:2459.
[25] Russell GT, Gilbert RG, Napper DH. Macromolecules 1993;26:3538.
[26] Scheren PAGM, Russell GT, Sangster DF, Gilbert RG, German AL. Macromolecules 1995;28:3637.
[27] Russell GT. Aust J Chem 2002;55:399.
[28] Kanda A, Duval M, Sarazin D, Francois J. Polymer 1985;26:406.
[29] Russell GT. Macromol Theory Simul 1994;3:439.
[30] Clay PA, Gilbert RG, Russell GT. Macromolecules 1997;30:1935.
[31] Smith GB, Russell GT, Heuts JPA. Macromol Theory Simul 2003;12: 299.
[32] van Berkel KY, Russell GT, Gilbert RG. Macromolecules 2005;38:3214.
[33] Smith GB, Heuts JPA, Russell GT. Macromol Symp 2005;226:133.
[34] Seabrook SA, Pascal P, Tonge MP, Gilbert RG. Polymer 2005;46:9562.
[35] Clay PA, Gilbert RG. Macromolecules 1995;28:552.
[36] Strauch J, McDonald J, Chapman BE, Kuchel PW, Hawkett BS, Roberts GE, et al. J Polym Sci Part A Polym Chem Ed 2003;41:2491.
[37] Maeder S, Gilbert RG. Macromolecules 1998;31:4410.